

OC 674/ME 568 (2020)

Introduction to Turbulence

Instructors: Jim Moum, CEOAS x 7-2553
 moum@coas.oregonstate.edu
 Jim Liburdy, MIME x 7-7017
 liburdyj@oregonstate.edu

Text: A First Course in Turbulence
 H. Tennekes and J.L. Lumley, MIT Press, 1972

Course Evaluation:

Assignments (~5) – 50%
Final/midterm – 25% each

Meeting: T-TH 2:00 – 3:50pm

SCHEDULE:TUESDAY

March 31 Introduction/Ch 1 (JL)

April Energetics of turbulence/Ch 3 (JM)7

April 14 Vorticity Dynamics/Chapt. 3 (JL)

April 21 Effects of Buoyancy /Chapt. 3,4 (JM)

April 28 Effects of Buoyancy /Chapt. 3,4 (JM)

May 5 Midterm (covers weeks 1-4)

May 12 Wall Flows/Chapt. 5 (JL)

May 19 Geophysical Flows/Chapt. 4 (JM)

May 26 Spectral Dynamics/Chapt 8 (JM)

June 2 Turbulent Structures (JL)

Final –finals weekTHURSDAY

April 2 Kinematics of turbulence/Ch 2,3 (JM)

April 9 Energetics of turbulence /Ch 3 (JM)

April 16 Vorticity Dynamics /Ch 3 (JL)

April 23 Effects of Buoyancy /Chapt. 3,4 (JM)

April 30 Jets&Wakes/Chapt. 4 (JL)

May 7 Jets, wakes & wall Flows/ Chapt. 4-5 (JL)

May 14 Statistical Description/Chapt 6 (JL)

May 21 Spectral Dynamics/Chapt 8 (JM)

May 28 Turbulence Structures (JL)

June 4 Summary

Turbulence

BIBLIOGRAPHY

A first course in turbulence. H. Tennekes and J.L. Lumley, MIT press, 1972.

Turbulence. 2nd ed., J.O. Hinze, McGraw-Hill, 1975.

An Introduction to Turbulent Flow. J. Mathieu and J. Scott, Cambridge, 2000.

The structure of turbulent shear flow. 2nd ed. A.A. Townsend, Cambridge, 1976.

The theory of homogeneous turbulence. G.K. Batchelor, Cambridge, 1953.

The physics of fluid turbulence. W.D. McComb, Oxford, 1990 .

Turbulence. U. Frisch, Cambridge, 1995.

Turbulence and stochastic processes: Kolmogorov's ideas 50 years on. J.C.R. Hunt, O.M. Phillips, and D. Williams, eds. The Royal Society, 1991.

An introduction to turbulent flow, J. Mathieu and J. Scott, 2002

Turbulent Flow: Analysis, Measurement and Prediction, P.S. Bernard and J. Wallace, 2002

Boundary layers

Boundary layer theory. 7th ed., H. Schlichting, McGraw-Hill, 1979.

An introduction to boundary layer meteorology. R.B. Stull, Kluwer, 1988.

Other aspects

Hydrodynamic stability. P.G. Drazin and W.H. Reid, Cambridge, 1981.

Fluid Mechanics. P.J. Kundu, Academic, 1990.

Buoyancy effects in fluids. J.S. Turner, Cambridge, 1973.

Fluid dynamics for physicists. T.E. Faber, Cambridge, 1995.

Small Scale Processes in Geophysical Fluid Flows, Kantha & Clayson, Academic, 2000

The Turbulent Ocean, S.A. Thorpe, Cambridge, 2005

Some Basics

Conditions for Turbulence

Large Re; 3D flow features; Broad spectrum of scales....

Role of Re – force ratio, time ratio, length scale ratio....

Consequences of turbulence:

enhanced diffusion, mixing, dispersion, dissipation....

greater surface forces due to momentum transport

Analysis:

stochastic vs deterministic (N-S eqns)

chaos – “deterministic randomness” – each pt has a state condition so
“infinitely dimensional”

Proper modeling of physics of flow

turbulence stress & viscous stress

energy content

Scaling:

local invariance: $f(\text{local parameters})$, e.g. shear rates; size of eddy

local energy scales: fluctuating velocity/frequency

energy dissipation rates

Random Nature of Turbulence?

4

Random Nature of Turbulence

"Random" — if an event may, or may not, occur
(flipping a coin lands heads)
(velocity at a pt. having a specific
value). Event → consequence known?

Pope : random if something is not certain or impossible

Why does turbulence exist?

→ perturbations; system response
(pendulum when disturbed)
(note → this is not necessarily
random).

Sensitivity to perturbations → very acute as $Re \uparrow$

$$Re = \frac{UL}{\nu} = \frac{\rho UL}{\mu}; \text{ (viscous forces not as strong relatively).}$$

Chaos Theory — nonlinear phenomena.
(feeds on itself)

- slight changes in initial conditions
(or perturbations) → very diff. results
at later times.

- Been well studied & applied some
but mostly at low Re.

Local instability:

What are the parameters?

Transition mechanism?

Ratio of forces = ?

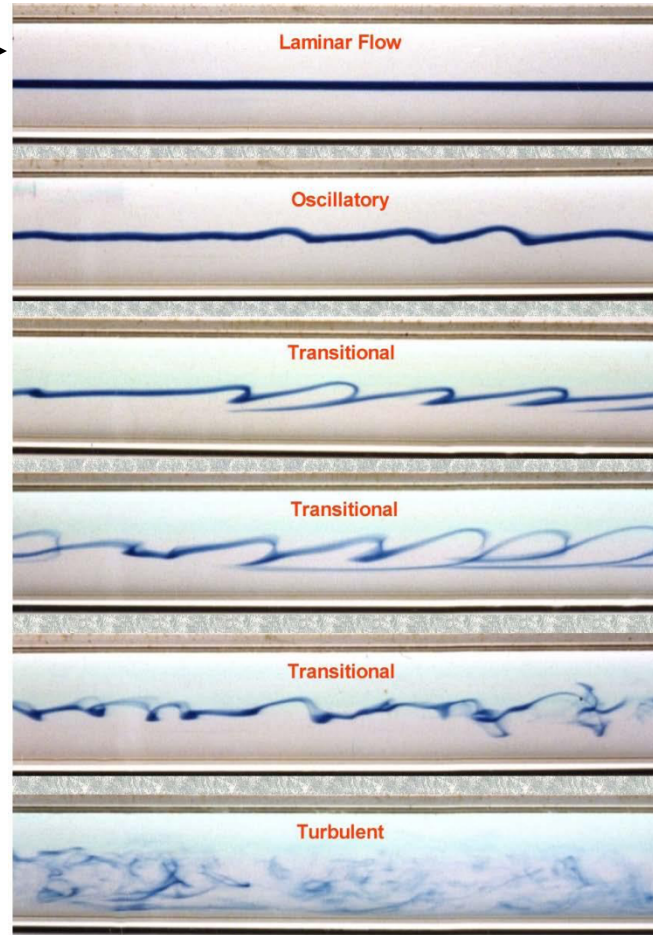
Growth rates of instabilities?

flow →

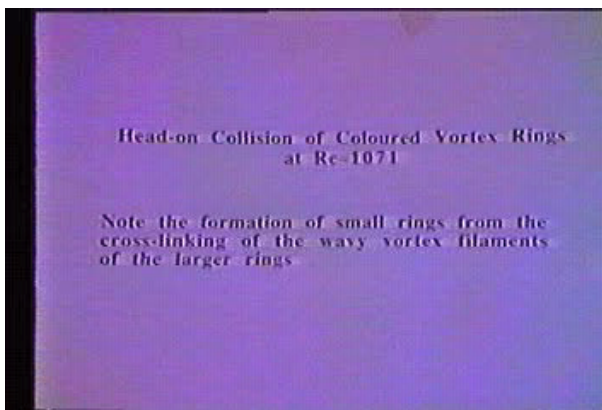
Kelvin-Helmoltz Instability



Instabilities



Increasing Re



Scaling

$$\tau_{\text{viscous}} \sim f(L, v) = L^2/v$$

$$\tau_{\text{convection}} \sim L/U$$

$$\tau_{\text{viscous}} / \tau_{\text{convection}} = Re_L$$

Consequence: Separation of scales

Large eddy scales: l

Small eddy scales: η

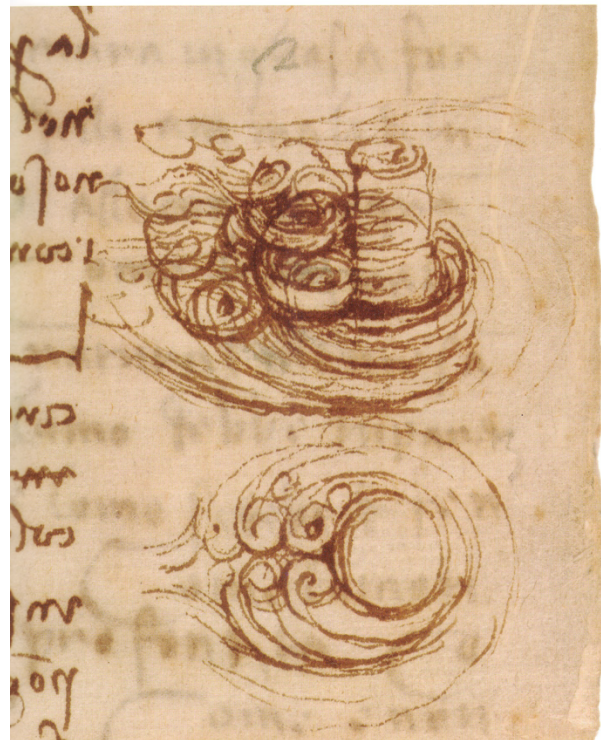
$$l \gg \eta \quad t_{\text{visc}} \gg t_{\text{conv}} : U > u \text{ (or } KE > ke)$$

If: Energy/m = Energy/pl³ ~ constant

Then: u decreases with decreasing length scale
(the local velocity scale decreases as l decreases)

therefore: largest scales have the most total energy

Viscosity ??



*Fluid mechanics is the paradise of the mathematical sciences
Because by means of it one comes to the fruits of mathematics*
da Vinci, 1452-1519

Example Flow Visualization illustrating Wide Scales of Motion: Da Vince Sketches

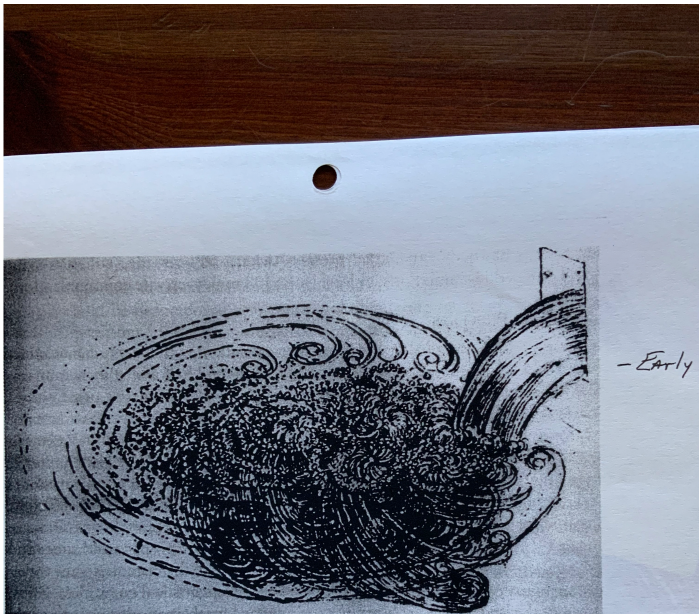
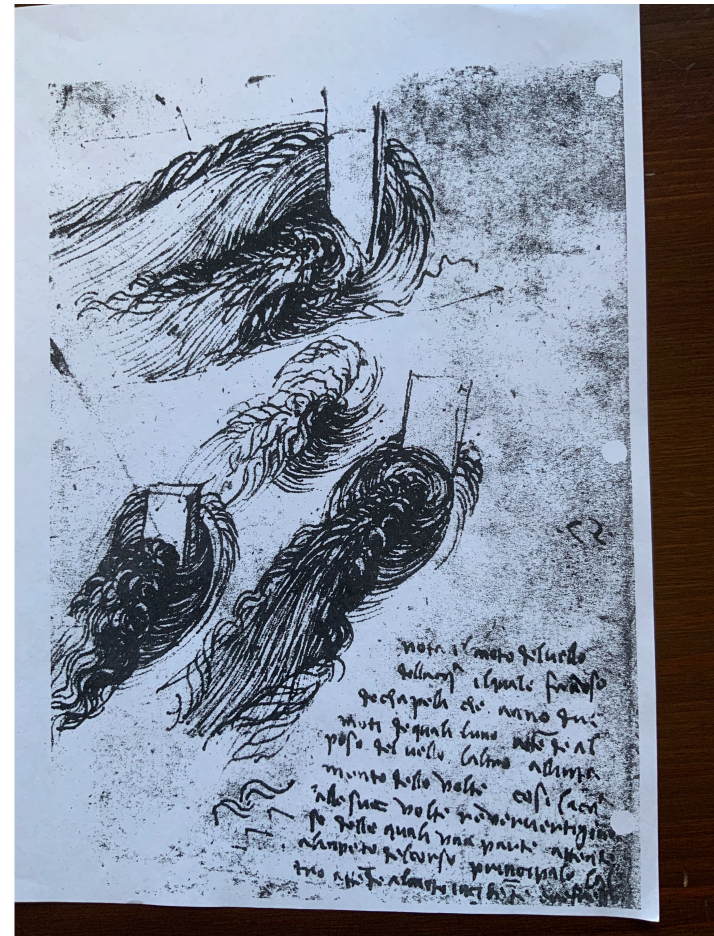


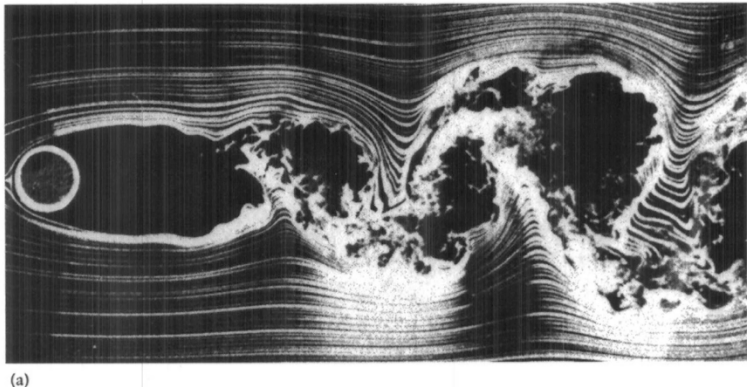
Figure 4.1: Leonardo da Vinci's sketch of water exiting from a square hole into a pool; circa 1500.

Mechanics is the paradise of the mathematical sciences because it is the science of the art of nature, and it is the source of knowledge of all the arts.

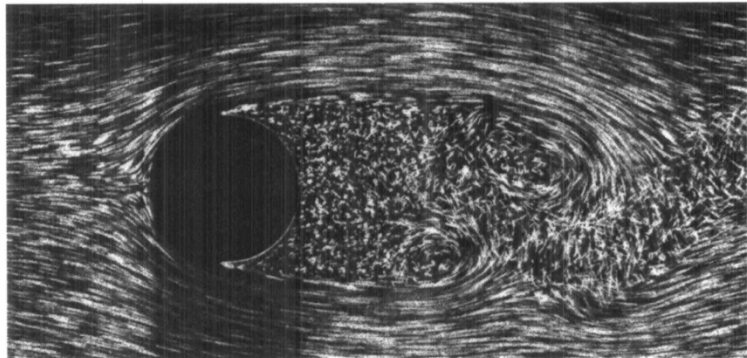
(Leonardo da Vinci, 1452–1519)



Separation of Scales



(a)



(b)

Figure 1.2. Visualizations of a turbulent cylinder wake; (b) shows a close-up. ((a) Courtesy of Thomas Corke and Hassan Nagib; (b) ONERA photograph, Werlé and Gallon (1972), reproduced with permission.)

Flow separation induces a high shear layer which becomes Unstable. This generates large scale flow structures which in turn generate smaller scale instability structures.

Navier Stokes

Nonlinear convection

$$\frac{\partial u_i}{\partial t} + u_j \frac{\partial u_i}{\partial x_j} = -\frac{1}{\rho} \frac{\partial P}{\partial x_i} + g_i + v \frac{\partial^2 u_i}{\partial x_j \partial x_j}$$

$$u_j \frac{\partial u_i}{\partial x_j} = \frac{\partial u_i u_j}{\partial x_j}$$

Other measures: $U_i = \overline{U}_i + u_i$ $\Omega_t = \overline{\Omega}_t + \omega_t$

MKE ($\overline{U}_i \overline{U}_i / 2$) tke ($\overline{u}_i \overline{u}_i / 2$):

Smallest scales: Kolmogorov scales

Smallest scales(η) $\sim f(v, \varepsilon)$

where ε = dissipation rate of kinetic energy (m^2/s^3)

idea: energy gain by smallest scales is from larger scales

$$\eta \sim (v^3/\varepsilon)^{1/4} \quad \tau_v \sim (v/\varepsilon)^{1/2} \quad v \sim \eta/\tau = (v\varepsilon)^{1/4}$$

$$\text{So: } Re_\eta = \eta v / v = 1$$

Scale ratios:

smallest scales versus “energy containing” scales:

if $Re_l = u l / v$ and $\varepsilon = u^2 / \tau_l$ then:

$$\tau_v / \tau_l = Re_l^{-1/2}$$

$$\eta / l \sim Re_l^{-3/4}$$

$$v / u \sim Re_l^{-1/4}$$

Separation of scales
as Re increases

?? As Re_l increases which scales change??

Energy Spectrum: $E = \text{energy/wavenumber}$

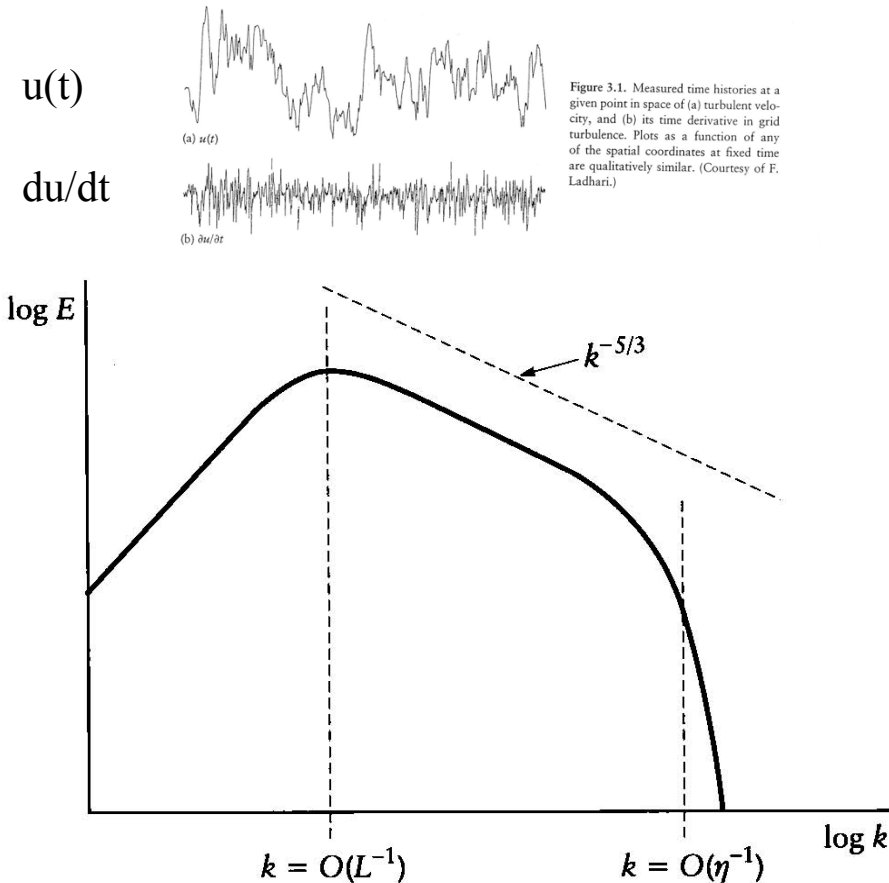


Figure 6.1. Sketch of the energy spectrum of turbulence in traditional log-log format, which brings out power laws as straight lines. The figure is drawn for a sufficiently high Reynolds number that there is a $k^{-5/3}$ inertial range, a feature we will address later in this chapter and in more detail in the next.

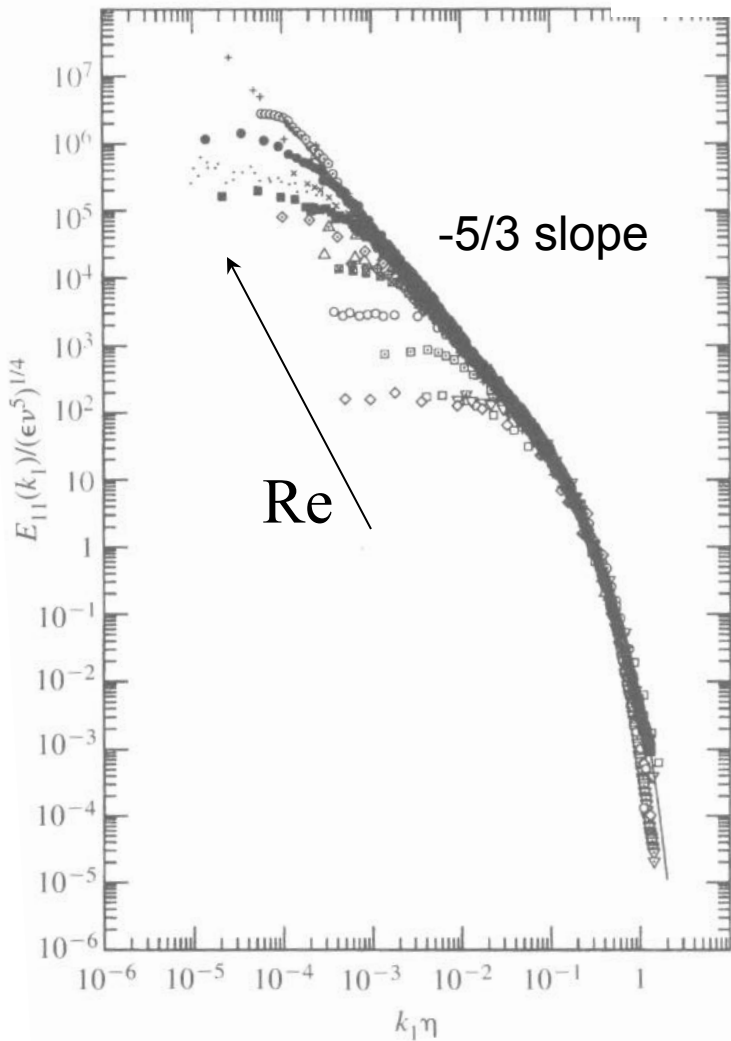
$$k = \text{wavenumber} \sim 1/l$$

$$\frac{1}{2} (u_i u_i) = \int_0^\infty E(k, t) dk$$

Dissipation rate of
turbulent kinetic energy

$$2\nu \frac{\partial u_i}{\partial x_k} \frac{\partial u_i}{\partial x_k}$$

Scaled Energy Spectrum



$$E_{11}(k_1)/(\epsilon v^5)^{1/4} \text{ vs } k_1 \eta$$

$E_{11}(k_1)$ - energy per wave number k_1
(subscript 1 denotes “1” directional component)

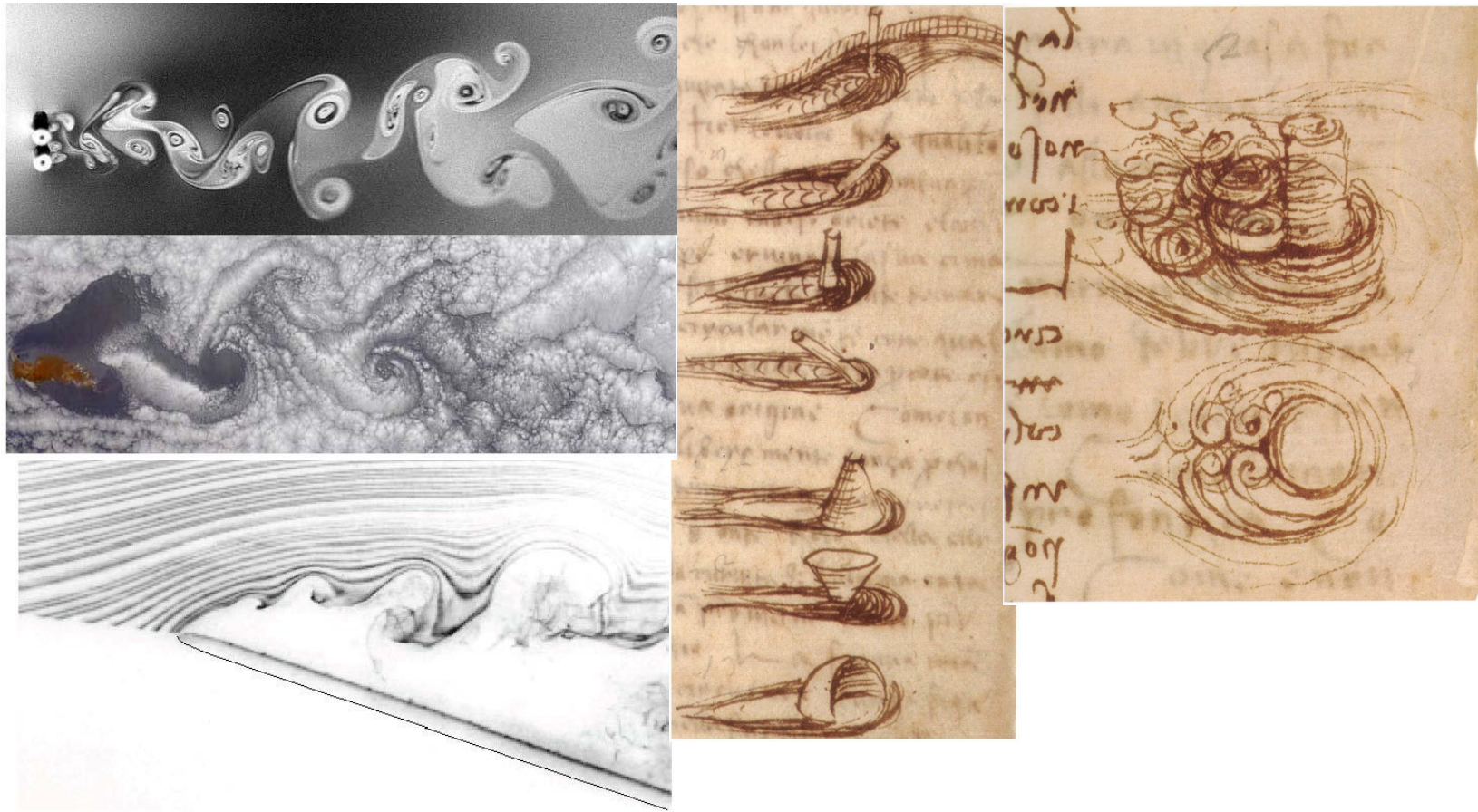
η – Kolmogorov length scale

ϵ - energy dissipation rate

v - viscosity

As Re increases scales separate

Large scale coherence: energy containing fluctuations



Law of the wall - scaled log velocity profile

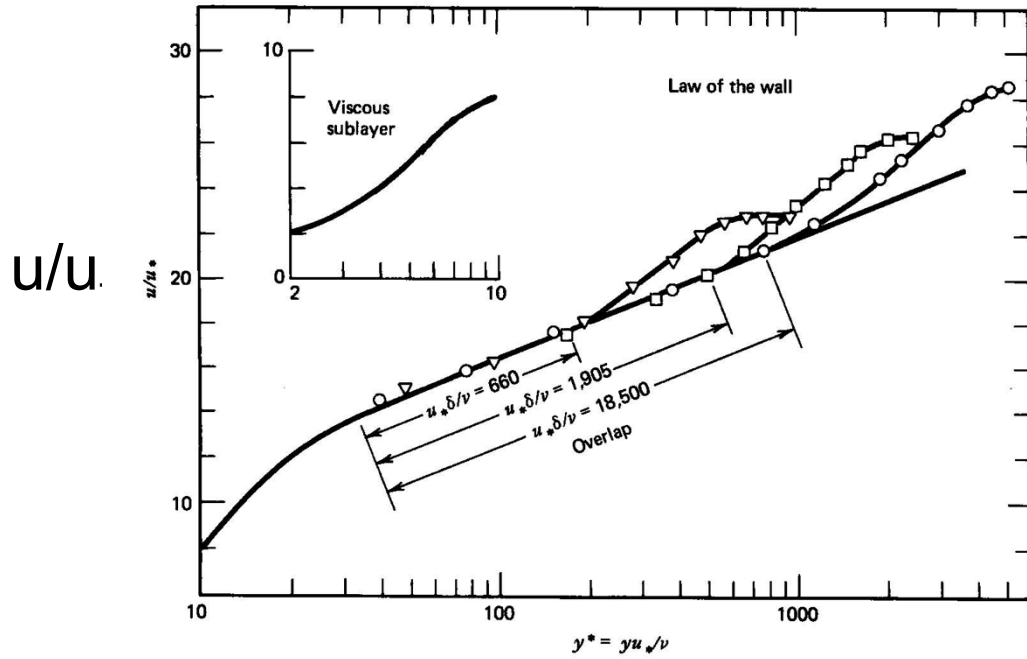


Figure 26.13 Composite velocity profiles for a turbulent boundary layer with zero gradient.

Patton, 3rd ed. 2005

$$u_T = (\tau_w / \rho)^{1/2} \quad y^+ = yu_T / \nu$$

Viscous layer:
 $y^+ : 0-5 \quad u^+ = y^+$

Buffer layer:
 $y^+ : 5-30$

Overlap:
 $y^+ : \log \text{region}$

$$y_{\log}^+ = 0.15 Re_T$$

$$Re_T = u_T \delta / \nu$$

Modifications: pressure gradient

Videos of wall turbulence & shear layer structures

- [https://gfm.aps.org/meetings/
dfd-2017/59b29bdbb8ac316d38841ad1](https://gfm.aps.org/meetings/dfd-2017/59b29bdbb8ac316d38841ad1)
-
- [https://gfm.aps.org/meetings/
dfd-2017/59bbd22bb8ac316d38841fe1](https://gfm.aps.org/meetings/dfd-2017/59bbd22bb8ac316d38841fe1)

Shear instability

transition mixing reaction rates

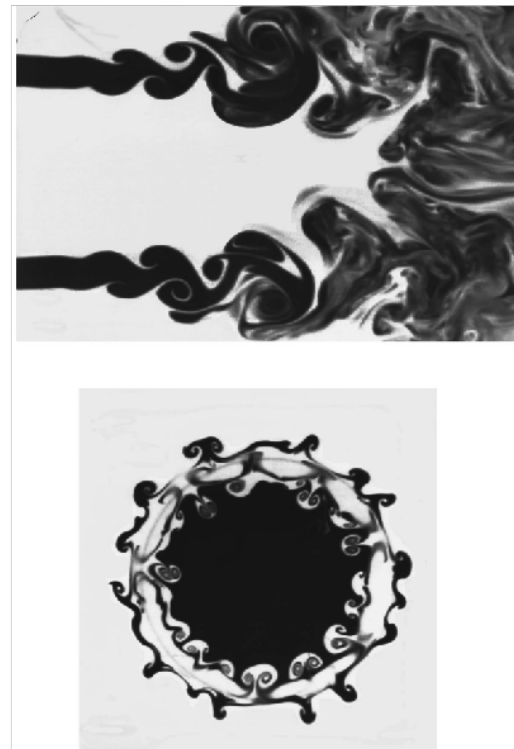


FIG. 1.

SHEAR INSTABILITIES IN THE NEAR FIELD OF COAXIAL JETS

**Submitted by E. Villermaux, H. Rehab,
and E. J. Hopfinger
(LEGI-CNRS, Institut de Mécanique de Grenoble,
BP 53X, 38041 Grenoble Cedex, France)**

Snapshots of the destabilization of a slow round jet (velocity u_1) by a fast coflowing annular jet (velocity u_2) in water with $u_2/u_1 = 3$ as manifested by the mixing of a high Schmidt number dye are shown. The Reynolds number based on the outer diameter and velocity $Re = u_2 D_2 / \nu$ is 2×10^5 . The wavelength λ_l of the longitudinal shear instability at the interface between the two streams (top picture, outer jet seeded) is about six times the vorticity thickness δ of the fast stream velocity profile at the lip of the annular tube, and the wavelength in the transverse direction λ_\perp (bottom picture, transverse cut perpendicular to the direction of the flow at

one inner diameter D_1 downstream of the exit plane) is about 3δ .

The development of the longitudinal and transverse instabilities is nearly concomitant and they both grow at the same rate. The longitudinal vortices from the transverse instability (mushroom-like structures on the bottom picture) connect rapidly the injection scale with the dissipative scale, resulting in an efficient mixing in the near field. The overall entrainment process is completed at a distance $[6/(u_2/u_1)]D_1$ downstream of the injection plane.¹

When the velocity ratio is further increased beyond about 8, a transition to an unsteady, wake-type recirculation regime is observed.^{1,2} The recirculation bubble oscillates periodically with a low frequency f , distinct from the jet mode, characterized by a Strouhal number based on the inner diameter and the outer velocity fD_1/u_2 of the order of 0.035.

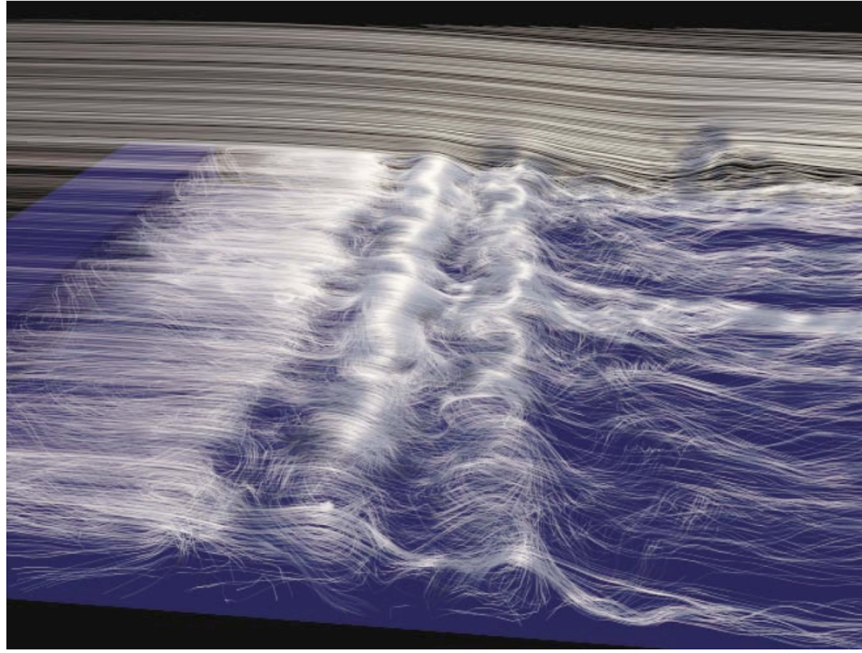


FIG. 1.

Coherent Structures in a Transitional Flow around a Backward-Facing Step

Submitted by

Tino Weinkauf and Hans-Christian Hege, Zuse Institute Berlin (ZIB)

Bernd R. Noack, Michael Schlegel, and Andreas Dillmann, Technical University Berlin

The transitional flow around a backward-facing step is visualized using illuminated streamlines of a snapshot (Fig. 1). The flow separates at the corner of the step. The resulting shear layer rolls up in two Kelvin–Helmholtz vortices. In the downstream direction, the streamlines form bundles due to secondary streamwise vorticity. The fluid experiences a small backward flow in the upstream region below the shear layer. The flow field is obtained from a large-eddy simulation by Kaltenbach and Janke at a Reynolds number of $Re_H=3000$ based on oncoming velocity and on step height. The corresponding boundary conditions are described in Ref. 1.

The streamlines are illuminated in order to enhance the

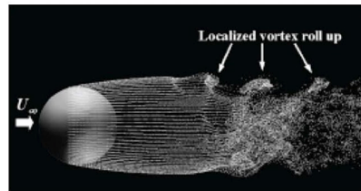
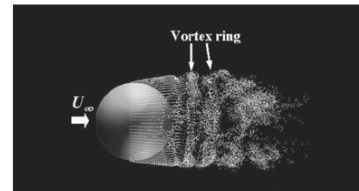
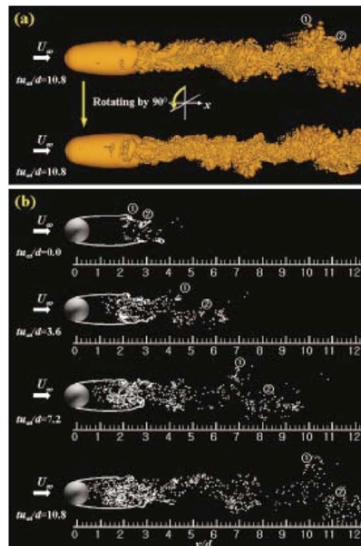
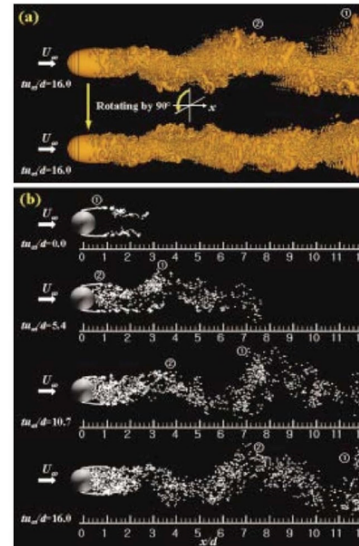
three-dimensional perception of the scene. This highly interactive, hardware-supported technique is described by Stalling, Zöckler, and Hege.²

The seeding of the streamlines is based on the mean curvature of surfaces which are locally perpendicular to the velocity field. As shown in Ref. 3, the mean curvature converges to infinity only near critical points of the considered vector field and vanishes in uniform flow. The mean curvature parametrizes a probability distribution used for seeding. Thus, streamlines passing only through regions of nearly uniform flow are blended out whereupon streamlines connected to critical points are emphasized. Additional streamlines are placed in a background slice in order to show how the coherent structures are embedded in the base flow.

¹H.-J. Kaltenbach and G. Janke, “Direct numerical simulation of flow separation behind a swept, rearward-facing step at $Re_H=3000$,” *Phys. Fluids* **12**, 2320 (2000).

²D. Stalling, M. Zöckler, and H.-C. Hege, “Fast display of illuminated field lines,” *IEEE Trans. Vis. Comput. Graph.* **3**, 118 (1997).

³T. Weinkauf and H. Theisel, “Curvature measures of 3D vector fields and their applications,” *J. Winter School of Computer Graphics* **10**, 507 (2002).

FIG. 1. $\text{Re}=3700$.FIG. 2. $\text{Re}=10^4$.FIG. 3. $\text{Re}=3700$.FIG. 4. $\text{Re}=10^4$.

Turbulent Flow past a Sphere at $\text{Re}=3700$ and 10^4

Submitted by
Giwoong Yun, Haecheon Choi, and Dongjoo Kim,
 Seoul National University, Korea

Large eddy simulation of turbulent flow over a sphere is conducted at the Reynolds numbers of 3700 and 10^4 based on the freestream velocity u_∞ and the sphere diameter d using an immersed boundary method.¹ Vortical structures are represented by the particle tracing and vortex identification methods.²

Figures 1 and 2 show the vortex rollup in the shear layer at $\text{Re}=3700$ and 10^4 , respectively. For $\text{Re}=3700$, vortices roll up locally in the azimuthal direction near the end of the

shear layer, whereas vortex rings are formed right behind the sphere for $\text{Re}=10^4$.

Figures 3(a) and 4(a) show the instantaneous vortical structures, respectively, at $tu_\infty/d=10.8$ ($\text{Re}=3700$) and 16.0 ($\text{Re}=10^4$) using the vortex identification method.² One can clearly notice that at this instant alternating vortical structures exist in one plane but do not appear in the perpendicular plane. Time traces of vortical structures using the particle tracing [Figs. 3(b) and 4(b)] show that this wake waviness is closely associated with the shear-layer vortical evolution. That is, the vortices, ① and ②, that are generated by the shear-layer instability persist in the far-downstream locations, resulting in the waviness of the wake structure.

¹J. Kim, D. Kim, and H. Choi, *J. Comput. Phys.* **171**, 132 (2001).

²J. H. Jeong and F. Hussain, *J. Fluid Mech.* **285**, 69 (1995).

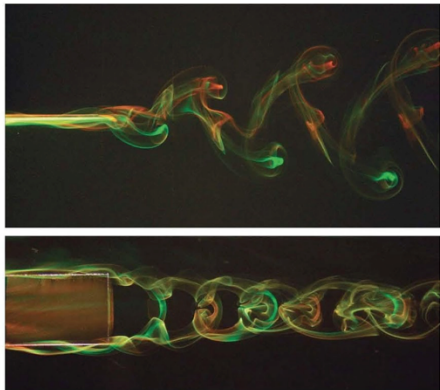


FIG. 1.

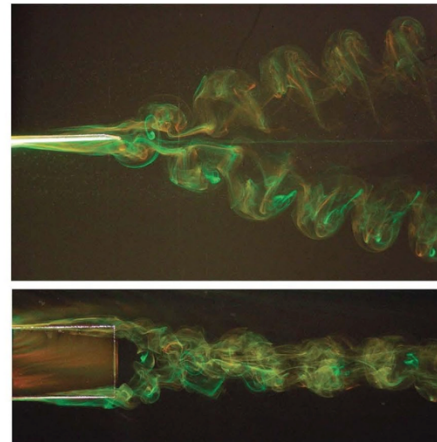


FIG. 3.

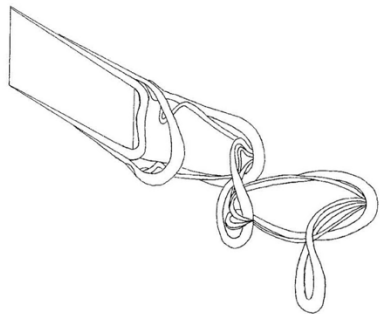


FIG. 2.

Wake of a low aspect ratio pitching plate

James H. J. Buchholz and Alexander J. Smits
Princeton University, Princeton, New Jersey 08544
 (Received 14 March 2005; published online 26 August 2005)
 [DOI: 10.1063/1.1942512]

A rigid plate of aspect ratio $S/C=0.54$ (S =span, C =chord) is pitched in a uniform flow about its leading edge. The double-amplitude to span ratio is $A/S=0.31$. The leading edge is hinged to the trailing edge of a stationary symmetric two-dimensional airfoil. Fluorescent dyes are introduced through a series of holes on each side of the airfoil support. The Reynolds number based on the chord of the plate and the freestream velocity U is 640.

Different flow regimes can be identified based on the Strouhal number, $St=fA/U$ (f =pitching frequency). Twice in each flapping cycle, a horseshoe vortex is created, consisting

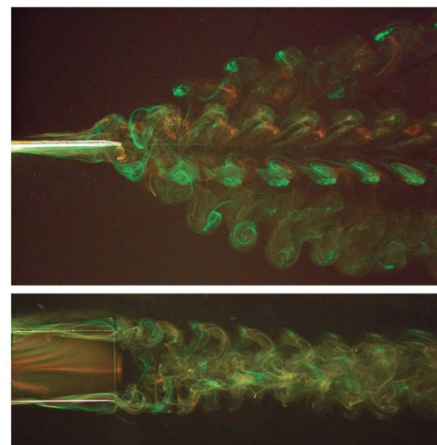


FIG. 4.

of vorticity shed by the top, bottom, and trailing edges. At $St=0.23$ (Fig. 1) the legs of each vortex loop are entrained by the tip of the subsequent loop forming a chainlike structure illustrated in Fig. 2. At $St=0.43$ (Fig. 3), the shed vorticity splits and forms two distinct branches. At $St=0.64$ (Fig. 4), some of the vorticity is rearranged to form additional hairpin loops that convect outward in the spanwise direction.

Studying such wakes is believed to be important for understanding the mechanisms of thrust production in fishlike swimming.

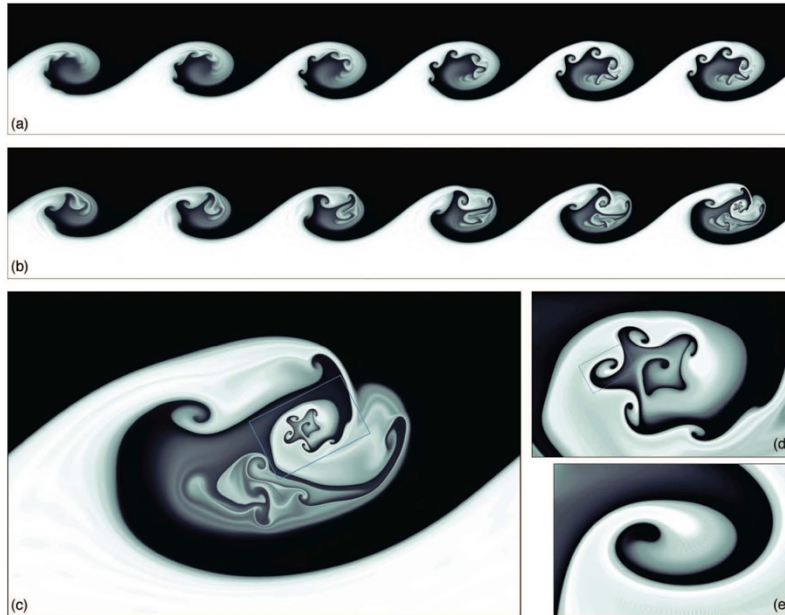


FIG. 1. (Color) Temporal development of the secondary (a) and the tertiary (b) Kelvin–Helmholtz instabilities. Successive closeups on the Kelvin–Helmholtz billows [(c)–(e)]. All pictures display the flow density field.

Fractal Kelvin–Helmholtz breakdowns

Jérôme Fontane,^{1,a)} Laurent Joly,¹
and Jean N. Reinaud²

¹Université de Toulouse, ISAE, F-31055 Toulouse, France

²School of Mathematics and Statistics, University of St Andrews,
St Andrews KY16 9SS, United Kingdom

(Received 21 July 2008; published online 25 September 2008)

[DOI: 10.1063/1.2976423]

The Kelvin–Helmholtz billow developing in an infinite-Schmidt number mixing layer at $Re=1500$ between two density-contrasted fluids (i.e., $\rho_{\text{black}}/\rho_{\text{white}}=3$) experiences a two-dimensional shear instability. Secondary Kelvin–Helmholtz billows are seen to emerge on the light side of the primary structure, and then are advected towards the core of the main billow as the wave overturns [Fig. 1(a)]. Due to the inertial baroclinic vorticity production, the braid region turns into a sharp vorticity ridge holding high shear levels and is thus sensitized to the Kelvin–Helmholtz instability.¹ We carry out numerical simulations of the temporal development

of the secondary mode when the flow is seeded at $t=18$ with the perturbation obtained from a linear stability analysis of the primary billow.²

If seeded earlier at $t=13$, the secondary instability develops on a longer wavelength. The larger central secondary billow breaks up in ternary rollups due to the same mechanism as the previous generation [Fig. 1(b)]. The self-similarity of the density pattern down the scales [Figs. 1(c)–1(e)] prefigures a two-dimensional route to turbulence through a fractal process.

The thinning of the density-gradient layer due to the successive folding of the Kelvin–Helmholtz billows is not compensated by mass diffusion. The corollary of the isovolume stretching is the development of the density field on increasingly smaller scales. This numerical challenge is solved by an adaptive mesh refinement leading to a considerable increase of the spatial resolution up to 10000×10000 .

^aPresent address: School of Mathematics and Statistics, University of St Andrews.

¹J. N. Reinaud, L. Joly, and P. Chassaing, “The baroclinic secondary instability of the two-dimensional shear layer,” *Phys. Fluids* **12**, 2489 (2000).

²J. Fontane and L. Joly, “Stability of the variable-density Kelvin–Helmholtz billow,” *J. Fluid Mech.* **612**, 237 (2008).

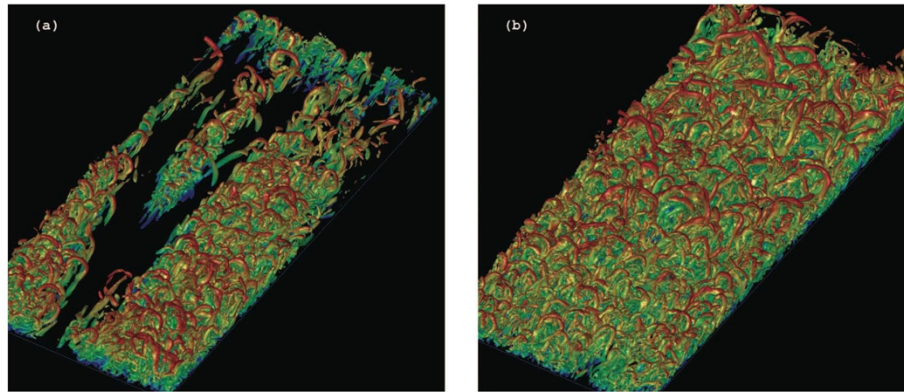


FIG. 1. (Color)

Forest of hairpins in a low-Reynolds-number zero-pressure-gradient flat-plate boundary layer

Xiaohua Wu^{1,a)} and Parviz Moin^{2,b)}

¹Department of Mechanical Engineering, Royal Military College of Canada, Kingston, Ontario K7K 7B4, Canada

²Center for Turbulence Research, Stanford University, Stanford, California 94305-3030, USA

(Received 17 July 2009; published online 11 September 2009)
[doi:10.1063/1.3205471]

The presence of hairpin shaped vortical structures in turbulent boundary layers has been postulated and pursued by a number of investigators over the past half century since the original work of Theodorsen in the 1950s.^{1–4} The availability of direct and large eddy numerical simulations in the 1980s provided more direct and statistical evidence in support of the presence of these structures in turbulent shear flows.^{5–8} Interestingly, vortical structures extracted by Robinson⁶ from Spalart's⁹ direct numerical simulation database of a “modeled” boundary layer were not consistent with the postulated dominance of hairpin structures. However, none of the previous simulations were of a genuine spatially developing turbulent boundary layer.

We have recently taken a Blasius layer from $Re_\theta = 80$ through transition to 1000 in a well controlled manner.¹⁰ Mean and second-order turbulence statistics are in very good agreement with classic experimental data. The instantaneous flow fields in both the transitional [Fig. 1(a)] and in the turbulent [Fig. 1(b)] regions are vividly populated by hairpin

vortices. This is the first time that direct evidence (in the form of a solution of the Navier-Stokes equations, obeying the statistical measurements, as opposed to synthetic superposition of the structures) shows such dominance of these structures. Additionally, hairpin packets arising from upstream fragmented structures are found to be instrumental in the breakdown of the boundary layer bypass transition. The persistence of the present hairpin forest into higher Reynolds number regions and its sensitivity to the route of transition require further investigation.

This work was supported by the U.S. Department of Energy, Canada Research Chair Program, and NSERC.

^aM. R. Head and P. Bandyopadhyay, “New aspects of turbulent boundary layer structure,” *J. Fluid Mech.* **107**, 297 (1981).

^bR. J. Adrian, C. D. Meinhart, and C. D. Tomkins, “Vortex organization in the outer region of the turbulent boundary layer,” *J. Fluid Mech.* **422**, 1 (2000).

³A. E. Perry and M. S. Chong, “On the mechanism of wall turbulence,” *J. Fluid Mech.* **119**, 173 (1982).

⁴I. Marusic, “On the role of large-scale structures in wall turbulence,” *Phys. Fluids* **13**, 735 (2001).

⁵P. Moin and J. Kim, “The structure of the vorticity field in turbulent channel flow. Part I. Analysis of instantaneous fields and statistical correlations,” *J. Fluid Mech.* **155**, 441 (1985).

⁶S. K. Robinson, “Coherent motion in the turbulent boundary layer,” *Annu. Rev. Fluid Mech.* **23**, 601 (1991).

⁷M. M. Rogers and P. Moin, “The structure of the vorticity field in homogeneous turbulent flows,” *J. Fluid Mech.* **176**, 33 (1987).

⁸M. J. Lee, J. Kim, and P. Moin, “Structure of turbulence at high shear rate,” *J. Fluid Mech.* **216**, 561 (1990).

⁹P. R. Spalart, “Direct simulation of a turbulent boundary layer up to $Re_\theta = 1410$,” *J. Fluid Mech.* **187**, 61 (1988).

¹⁰X. Wu and P. Moin, “Direct numerical simulation of turbulence in a nominally-zero-pressure-gradient flat-plate boundary layer,” *J. Fluid Mech.* **630**, 5 (2009).

^aElectronic mail: xiaohua.wu@rmc.ca.

^bElectronic mail: moin@stanford.edu.

Turbulence by R.W. Stewart

<http://web.mit.edu/html/ncfmf.html>